IAC-09-A6.1.04

OPTICAL SURVEYS FOR SPACE DEBRIS IN MEO – SIMULATIONS AND FIRST RESULTS

T. Schildknecht

Astronomical Institute, University of Bern, CH-3012 Bern, Switzerland
thomas.schildknecht@aiub.unibe.ch

T. Flohrer[1], A. Vananti[2]

[1]ASRO at ESA ESOC, Robert-Bosch-Strasse 5, 64293 Darmstadt, Germany
[2]Astronomical Institute, University of Bern, CH-3012 Bern, Switzerland

ABSTRACT

During the last decades considerable effort has been spent to measure the space debris environment in different orbital regimes using radar and optical sensors. Most surveys concentrated either on the densely populated low Earth orbit altitudes (LEO) or on the unique region of the geostationary ring (GEO). Some limited results from surveys of the geostationary transfer region (GTO) are available, as well. The increasingly populated space used by the global navigation satellite constellations like GPS, GLONASS, Beidou-2/COMPASS, and GALILEO has not been systematically investigated so far. Compared to the GEO/GTO surveys, MEO survey strategies have to cover much larger ranges of angular velocities and orbit inclinations. Furthermore, due to the large volume occupied by these constellations the apparent surface density of objects in the survey space is expected to be low and therefore the generation of statistically relevant results requires a large area to be surveyed. The paper will present MEO survey strategies for two sensors - the ZimSMART wide field telescope located at the Zimmerwald observatory in Switzerland, and the ESA space debris telescope having a narrow field of view. The performance in terms of population coverage and orbit recovery will be evaluated for a particular observation scenario and a simulated breakup debris population.

INTRODUCTION

The most densely populated orbital region above 2000 km altitude is clearly the geostationary ring (GEO). More than 1180 large objects are known to orbit in this region. Over 380 of these are controlled, active spacecraft [1]. Consequently efforts to investigate the small-size debris environment at high altitudes were mostly focused on the GEO region. Space debris surveys revealed a significant number of previously unknown debris in GEO including a number of clusters in the orbital element space. Two of these clusters are associated with known breakup events, and the others are most likely the result from unnoticed breakups. Currently the observations indicate a total of 5 to 10 breakup events in the GEO ring.

The medium Earth orbit region (MEO) used by global navigation satellite systems (GNSS) like GPS, GLONASS, Beidou-2/COMPASS, and GALILEO, on the other hand, has still a much lower spatial density of large, known objects. Less than 250 objects in MEO are currently listed in the USSTRATCOM catalogue. Although the overall spatial volume occupied by these satellite constellations is orders of magnitude larger than the GEO ring, the distribution in orbital element space is far from homogeneous. There are e.g. about 70 objects concentrated in a single GLONASS orbital plane. If we assume a similar breakup rate as in GEO, where the observations indicate 1-2 events per 100 objects in 25 years, we expect that one or two events could have taken place in MEO. A single event would easily produce more than 500 fragments larger than 10 centimeters in a rather confined region, i.e. a particular orbital plane of one of the constellations. These considerations motivated the development of observations scenarios for optical MEO surveys.

In order to study the performance of observation scenarios, a synthetic breakup population was generated. ESA's Program for Radar and Optical Observation Forecasting (PROOF) in the version 2005 [2] was then used to assess the performance in terms of coverage and orbit recovery.

TARGET FUNCTIONS

Designing observation scenarios requires first of all a clear understanding of the primary goals of the observations. In order to optimize observation scenarios for particular objectives we thus need a well-defined target function. This definition is often not obvious, as several 'competing' objectives may exist. In such cases the proper prioritization of these objectives is important. We assume that generally limited sensor and sensor network performance do not allow optimizing for all objectives simultaneously, and thus the objectives are 'competing'.

Surveys fall into two general categories: a) statistical surveys, and b) 'leak-proof' surveys. Statistical surveys aim at probing a population or a sub-population in a way that allows collecting statistical information on the population. A 'leak-proof' survey, on the other hand, attempts to detect all objects within given ranges of object parameters (e.g. larger than a given size and below a given altitude).

Leak-proof surveys do not automatically lead to a catalogue of objects. Cataloguing requires that the orbits of the objects can be determined. In particular an initial orbit must be determined and the quality of this orbit must be good enough, such that the object may be recovered (either by intentionally tracking the object or by correlating observations from further surveys). If cataloguing is not required, orbits may still be of interest. These so-called 'statistical orbits' may be more or less accurate, depending on the requirements. For some applications a moderately accurate location of the orbital plane (inclination and right ascension of the ascending node) in combination with the mean motion may be sufficient. Others may require further information on the eccentricity and the perigee. We may note that both, leak-proof and statistical surveys, may be designed to provide either statistical orbits or a catalogue of objects.

The search for small space debris represents a particular class of target functions. Optimizing surveys for the detection of small size objects is usually strongly confining the orbital element space for the detectable objects. Such surveys thus cover a sub-population only, in other words, suffer from considerable 'selection biases'.

OBSERVATION SCENARIOS: DESIGN PARAMETERS AND EXAMPLES

There is a multitude of parameters to be considered when designing observation scenarios. Some pertain to the individual sensors and the sensor network, others are related to the characteristics of the population to be surveyed. In addition we have to respect a variety of constraints. These are parameters,

System Characteristics	ZimSMART	ESASDT	Comments
Field of View	4.19°	0.7°	
Pixel size	4.95”	1.2”	
Object angular velocity	~30”/s	~30”/s	MEO
Exposure time	≤5s	≤2s	
Read/slew time	10s	18s	(settling time!)
Secondary Parameters			
Cycle time	15s	20s	
Field dwell time	503s	84s	
Pixel dwell time	0.17s	0.04s	(stars or object)
Trail length	30 pixel	50 pixel	(stars or object)
Observations/tracklet, 1 field	≤33.5	≤4.2	1-field fence
Observations/tracklet, 6 fields	≤5.6		6-field fence

Table 1: Sensor characteristics of the small-aperture, wide FoV sensor ZimSMART in Zimmerwald, and the ESA 1-meter telescope in Tenerife (ESASDT).

which are not subject to optimization by intention. Examples of such constraints could be the minimum galactic latitude of the survey fields or the maximum amount of moonlight allowed.

Essential design parameters are related to the particular detection technique to be used. Most detection algorithms require (implicitly or explicitly) a series of single detections of an object within a given time interval. For high-altitude orbits, i.e. in the GEO, GTO, or MEO region, this interval is typically of the order of a few minutes. The series of detections pertaining to a single object is called a ‘tracklet’. Tracklets thus contain a minimum of two observations. Usually more than two detections are required in order to reduce the false alarm rate.

The minimum number of objects per tracklet is a crucial design parameter for every observation scenario. The scenario must guarantee that this minimum of observations is acquired within the field of view (FoV) crossing time, or the so-called field dwell time. In other words the scenario must be designed for this minimum number of revisits of same field within the field dwell time. The field dwell time is also limiting the orbit arc length covered by the observations of a single tracklet. Field dwell times are given by the FoV diameter divided by the apparent angular velocities of the objects with respect to the survey field. If the survey field is fixed with respect to the stars, the angular apparent velocity is the apparent topocentric velocity with respect to an inertial system. Figure 1 shows the apparent topocentric angular velocities of MEO objects as a function of declination (inertial system). The figure contains all known objects in GPS and GLONASS orbits as seen from the Optical Ground Station (OGS) at Tenerife during the night of 20091221. Maximum apparent angular velocities are in the range of 30 to 36 arcseconds per second.

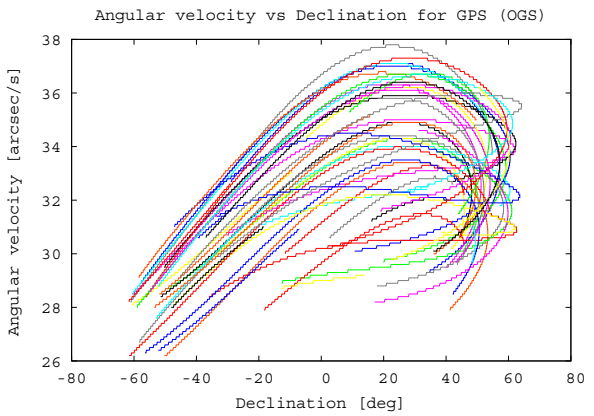

Figure 1: Apparent topocentric angular velocities of MEO objects as a function of declination (inertial system). All known objects in GPS and GLONASS orbits as seen from the OGS site during the night of 20091221 (DISCOS tle data set from May 2009).

Typical sensor characteristics of the small-aperture, wide FoV sensor ZimSMART, and the 1-meter ESA telescope (ESASDT) are given in Table 1. The field dwell times for MEO objects (30”/s angular velocity) are about 500s for ZimSMART and about 80s for the ESASDT, respectively. The number of exposures, which may be acquired during the field dwell time, is given by the cycle time, i.e. the time between consecutive exposures. As a result we get 33 exposures and 4 exposures per field dwell time, respectively. This is the number of observations per

tracklet, if we assume a single survey field (row labeled 'observations/tracklet, 1 field' in Table 2). Instead of acquiring 33 exposures per tracklet with ZimSMART we may survey several fields 'in parallel'. If we require at least three observations per tracklet, we may observe 6 fields in parallel with 5 exposures per tracklet (last row of Table 2). For ESASDT even two parallel fields would result in less than three observations per field. If the survey fields, which are observed in parallel, are adjacent to each other or even overlapping partially we call the resulting survey pattern a 'fence'.

Important design parameters are given by the population of objects to be observed. Apart from the apparent angular velocities, the apparent density of objects may be used to decide on where to place the survey fields. Figure 2 shows the apparent, geocentric paths of GPS satellites in the right ascension-declination system (inertial system). The circles indicate locations of special interest: three circles show areas where two orbital planes are crossing each other, the rightmost circle indicates the culmination region of an orbital plane. Crossing points are of interest because two orbital planes may be surveyed simultaneously at these points. On the other hand, the apparent paths of GPS satellites of one orbital plane tend to concentrate in a very small region at the culmination points.

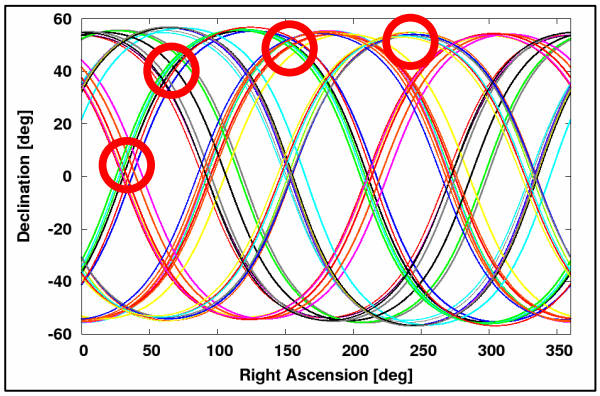

Figure 2: Apparent, geocentric paths of GPS satellites in the right ascension-declination system (inertial system). (24 hours on 20091221; DISCOS tle data set from May 2009). Note the one object crossing slightly outside the fence.

A particular survey fence for the GPS population is shown in Figure 3. The fence consists of 6 ZimSMART fields. Straight arrows indicate the apparent motion of the GPS objects. The curved arrows show the sequence of the exposures. This fence is 'leak proof' (for the crossing orbital planes) and will produce tracklets with 6 observations distributed over 500 seconds.

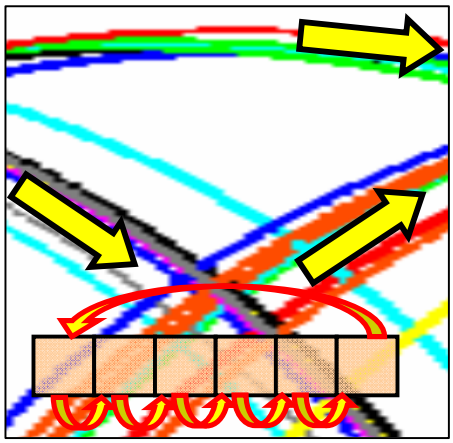

Figure 3: Horizontal survey fence at a crossing point of the GPS population (40° declination). The fence consists of 6 ZimSMART fields. Straight arrows indicate the apparent motion of the GPS objects. The curved arrows show the sequence of the exposures.

Sensor sensitivity considerations may require blind tracking (with the expected apparent velocity) of the object of interest during the exposures. In this case the survey must be optimized for a single orbital plane and crossing points may become of less interest. Figure 4 gives the apparent astronomical magnitudes of MEO objects at the distance of 25000km as a function of phase angle and object diameter (for a Bond albedo of 0.1). The survey fields may in most cases be selected in a way that the phase angles are smaller than 90°. Figure 4 may be used to determine the limiting objects sizes for given sensor and observing site parameters, and object angular velocities.

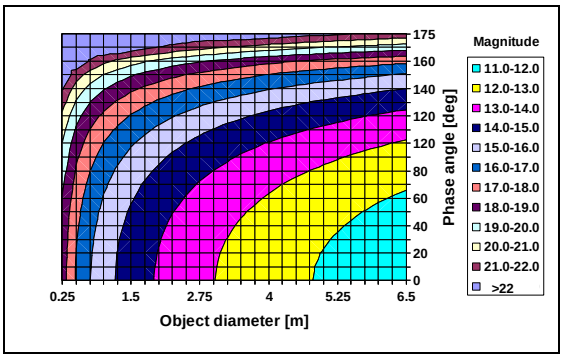

Figure 4: Magnitude as a function of phase angle and object diameter for a topocentric distance of 25000km (for a Bond albedo of 0.1).

SYNTHETIC POPULATION

The current MEO population of known objects does only contain intact spacecraft and upper stages. In GEO, however, several breakup events are known to have taken place and additional ones are suspected. We were therefore interested in the characteristics of a hypothetical breakup in MEO. For this purpose an explosion with isotropic ejection velocities of the fragments was simulated. The explosion model was taken from [3]. Figure 5 gives the distribution of the ejection velocities. The distribution of the orbital elements of the fragments was then analyzed. For the semimajor axis, the inclination, and the ascending node we assumed a Gaussian distribution and determined the corresponding standard deviation. The eccentricity showed an asymmetric distribution with a median value of about 0.03. For the argument of the perigee and the mean anomaly we assumed a uniform distribution.

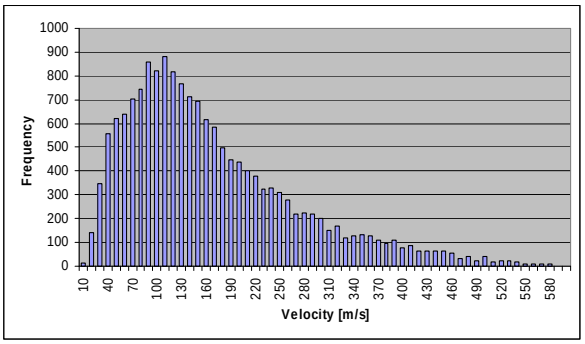

Figure 5: Distribution of ejection velocities.

All catalogued MEO objects could be potential explosion sources and we were interested in a synthetic population reflecting this fact. We therefore convolved the standard deviation of each orbital element of the explosion fragments with the standard deviation of the corresponding element of the catalogue population. Obviously this had to be done separately for each orbital plane.

Similarly the evolution of the orbital elements of the GPS and the GLONASS population was analyzed. The dispersion of the orbital elements over a time interval of 20 years was again characterized in terms of standard deviations. Finally the dispersions due to evolution and the standard deviations of the explosion fragments (convolved with the standard deviations of the catalogue distribution) were combined by forming the quadratic sums. Table 2 gives the resulting standard deviations for the semimajor axis, the eccentricity, the inclination, and the right ascension of the ascending node. These values were eventually used to generate synthetic populations of 1000 objects for each (nominal) orbital plane of the GPS and the GLONASS constellations.

	σ expl	**σ evol**	**σ tot**
a [km]	1220	~ 0	1220
Eccentricity	0.02	0.01	0.022
inclination [°]	1.5	0.5	1.58
RAAN [°]	5	5	7

Table 2: Standard deviations of the distribution of the semimajor axis, the eccentricity, the inclination, and the right ascension of the ascending node (RAAN) for the explosion fragments convolved with the catalogue population (σ expl), the orbital evolution (σ evol), and the quadratic sum of the two (σ tot).

SIMULATION OF A SURVEY SCENARIO

A simulation of a survey scenario is required to assess two key parameters of a survey strategy: the coverage of a reference population, and the quality of the orbit determination. The latter is in particular relevant for the qualification of "survey only" strategies.

In our example we select a first survey area close to crossing points of orbital planes, and a second survey area close to the expected position of objects in one selected orbital plane 1 hour after the crossing of the first area.

Figure 6 gives the topocentric center coordinates of the FoV for the two subsequently executed surveys: survey fence t_0 and survey fence t_1, each fence consisting of 9 fields and being observed for 1 h each. The added trajectories of exemplary objects of the reference population illustrate the observation conditions. Statistically, we may expect ~ 1/12 of the population of a selected orbital plane to cross a 1h survey fence. We here use a sample of 1000 objects of the synthetic population. As this population is grouped into equally sized 10 classes of orbital planes, we may expect for our sample that ~8 objects per hour cross the survey fences.

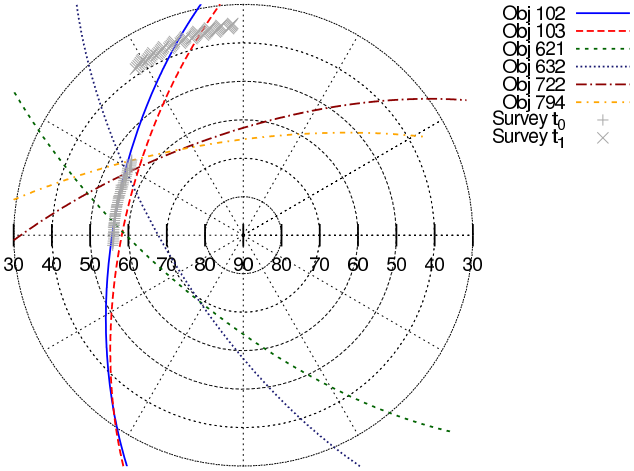

Figure 6: Topocentric right ascension (North=right) and declination for Zimmerwald of the FoV center coordinates in a combined survey scenario (1h survey fence t_0, followed by 1h survey fence t_1), combined with trajectories of sample objects.

We use ESA's Program for Radar and Optical Observation Forecasting (PROOF) in the version 2005 [2] for the simulation of the survey strategies. PROOF-2005 is provided with a plug-in interface that allows outputting the observation geometry for all so-called "crossing" objects. We make use of this function to simulate realistic observations in right ascension and declination and to add realistic noise. This allows simulating the first orbit determination with external tools. We further extensively use PROOF-2005's automation option, which makes it possible to simulate the frequent changes of the orientation of the sensor pointing. In order to extend the statistical relevance, we extend the simulation of the survey so that both fences are observed for uninterrupted 12h, which assumes that two sensors operate in parallel.

The detection algorithm in PROOF-2005 remains disabled, as we are not interested in evaluating the capabilities and limits of a specific instrumentation, but in the number of crossing objects in a given FoV. We fix the FoV diameter to 3 deg, as it is a typical value for medium aperture, wide FoV sensors.

Each fence is simulated to consist of 9 non-overlapping fields. This number is close to the maximum for a 3 deg sensor FoV, if a minimum of 3 observations per tracklet has to be ensured.

Figure 7 shows the coverage of the target population in both surveys, t_0 and t_1. The simulation gives for survey fence t_0 a total crossing of 1185 crossing events, which relate to 9 objects with only one crossing event, and 172 objects with more than one crossing event. The average number of crossings events per object (if it is not a unique crossing event) is 6.837. Survey fence t_1 shows 488 crossing events, relating to 2 uniquely crossing objects and 138 objects with multiple crossing events. For the survey fence t_1 the average number of crossings per object is 3.521.

Comparing the crossing event statistics for the two fences reveals that the first survey fence indeed allows covering more than one orbital plane. We may cover here 3 orbital planes. We further conclude that on average the minimum number of observations per tracklet is possible, even for the survey fence t_1.

One drawback of the first survey fence covering more than one orbital plane is the sub-optimal coverage of a specific orbital plane. Some objects may just "slip through", as it is the case for object 103 in Figure 6. A crossing event statistics that considers only the 100 objects of the orbital plane to be covered with survey fence t_1 provides some insight into this fact. A total of 4 objects have unique crossing events, and only 59 are found to have multiple crossing events. Hence, the coverage efficiency is about 59% for the first survey t_0. For the survey fence t_1, that is dedicated to cover the selected orbital plane, we do not find unique crossing events, but find 82 objects with multiple crossing events. The coverage efficiency is 82% for this survey fence placed 1 h behind the first survey fence t_0. This in turn means that about half of the population of the orbital plane (that was selected by placing the survey fence t_1) can be covered sufficiently.

A large room for further studies leaves the question, how many sensors are required, and how these sensors shall be scheduled, in order to cover most efficiently more than one selected orbital plane. Special attention should be paid to finding optimal strategies of combining survey results from subsequent nights, mainly if a low number of sensors does not cover a selected survey fence continuously.

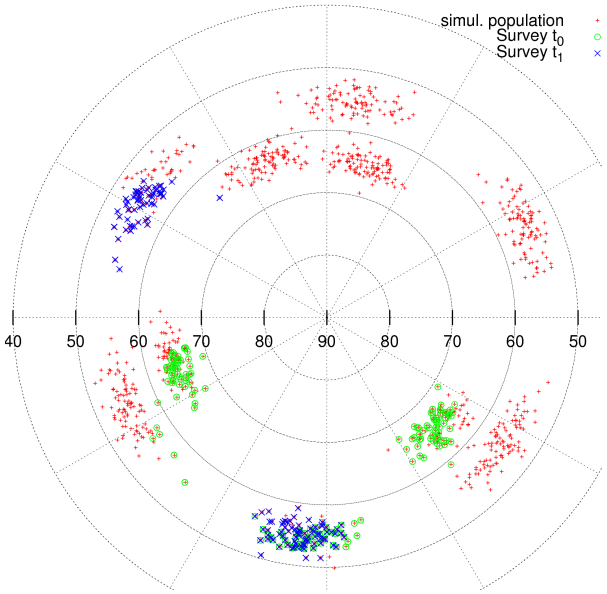

Figure 7: Orbital poles (right ascension of ascending nodes vs. inclination) of a reference population, and the possible detections in a combined survey of two fences (continuous coverage over 12h for each fence).

We continue our discussion with an assessment of the quality of the initial orbit determination for selected objects crossing the survey fences t_0 and t_1.

The orbit determination software ORBDET, that is part of the CelMech program system [4], has been extended to support the simulation of observations from PROOF's plug-in output. ORBDET now allows adding normal-distributed noise to the two observables right ascension (RA) and declination (as function of *cos*(RA)). This "astrometric" noise may be considered to represent to the first order the sum of epoch registration noise, and position measurement (centroiding) noise. When related to the parameters of optical sensors, the astrometric noise is often quoted to be "1/10 of a pixel", so for a pixel scale of 2"/pixel we would expect an astrometric noise of 0.2". While this 1/10 of a pixel is applicable as a rule-of-thumb to narrower FoV diameters, it is unknown so far, whether this rule is similarly applicable for the planned survey sensors with a wide FoV.

We selected ORBDET's boundary value method to determine a first orbit from a short arc of about 1min, by searching for minima in the 250 - 60000 km range, followed by an orbit improvement step using all simulated observations and considering perturbations from the Earth oblateness (J2) and luni-solar perturbations.

We present here the orbit determination results for two exemplary objects that cross the survey fences t_0 and t_1. Figure 8 and Figure 9 show that for realistic astrometric noise levels (i.e. below 2") the first orbit determination provides promising results. Both, the orientation of the orbital plane, and the shape of the orbit are correctly determined with only very minor deviations to the "true" values provided by PROOF.

However, the analysis of this aspect has just started and further studies are required. It is important to note that the question how observations between the two surveys fences are correlated is not addressed here. We just assume that a correlation is always possible and ambiguous cases can be resolved.

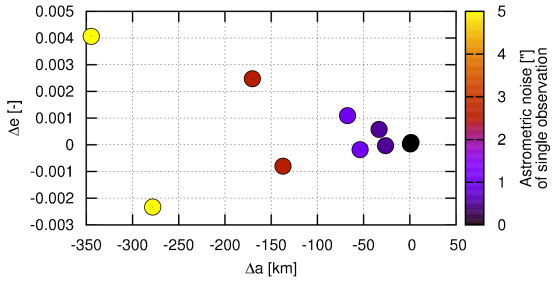

Figure 8: Differences (simulated orbit in PROOF vs. the determined orbit) in semi major axis (a) and eccentricity (e) as a function of the simulated astrometric noise.

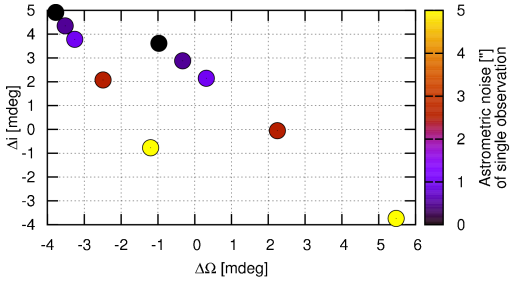

Figure 9: Differences (simulated orbit in PROOF vs. the determined orbit) in right ascension of ascending node (Ω) and inclination (i) as function of the simulated astrometric noise. NB: the orbital elements for simulated objects in PROOF are given with 2 digits (10 mdeg precision) only, this plots basically shows that we obtain a perfect match for all considered astrometric noise levels.

Further work in simulating the survey scenarios shall also address the radiometric performance for selected sensor architectures, together with the analysis of the survey performance if instrumental constraints are applied. PROOF with its link to ORBDET shall be utilized to discuss the orbit determination of the selected strategies. According to

the target functions it is the goal to find optimal layouts of survey fences and of the scheduling sequences for both, the statistical sampling, and the leak-proof maintenance of a catalogue of orbital elements. At least the visibility of survey fields, the temporal spacing of individual observations (that might be important drivers for correlation and orbit determination algorithms), and the number and distribution of survey sensors need to be considered. We always assume, however, that the problem of correlating individual detections of identical objects between survey fences, thus likely also between several (distributed) survey sensors, is solved.

SUMMARY AND CONCLUSIONS

The MEO region is becoming increasingly populated by navigation satellite constellations. Although the spatial density of the known population is still low, compared to other regions, a single breakup event could change the situation substantially. If we apply the statistical GEO breakup rate, as derived from debris surveys, there is a high probability that an (unnoticed) breakup has already taken place in MEO.

Observation scenarios to survey the MEO region with optical telescopes were developed. In order to determine expected detection rates and to eventually study the performance of these scenarios, a synthetic breakup population was generated.

We implemented a simulation environment based on PROOF and ORBDET allowing to assess the survey performance in terms of coverage and (first) orbit determination quality, considering realistic noise levels.

First results for one selected survey strategy indicate that the orbit determination is feasible and leads to promising results. For the selected case of two combined 1 h survey fences (potentially requiring two telescopes that are not necessarily collocated) we show that up to half of the population in a selected orbital plane may be sufficiently covered.

REFERENCES

[1] Choc, R., R. Jehn, Classification of Geosynchronous Objects, Issue 11, ESA ESOC Space Debris Office, February 2009.

[2] Oswald, M., S. Stabroth, C. Wiedemann, H. Klinkrad, Upgrading ESA-PROOF, the Program for Radar and Optical Observation Forecasting, AMOS Technical Conference, Wailea, Hawaii, 2004.

[3] Pardini, C., L. Anselmo, Dynamical Evolution of Debris Clouds in Geosynchronous Orbit, Advances in Space Research, Vol. 35, Issue 7, pp 1303–1312, 2005.

[4] Beutler, G., T. Schildknecht, U. Hugentobler, and W. Gurtner, Orbit determination in satellite geodesy, Adv. Space Res., **31** (8), pp. 1853-1868, 2003.